Quantitative Fluorescence Microscopy: From Art to Science

Mark Fricker,[1] John Runions,[2] and Ian Moore[1]

[1]Department of Plant Sciences, University of Oxford, Oxford, OX1 3RB England; email: mark.fricker@plants.ox.ac.uk, ian.moore@plants.ox.ac.uk

[2]School of Biological and Molecular Sciences, Oxford Brookes University, Oxford, OX3 0BP England; email: jrunions@brookes.ac.uk

Annu. Rev. Plant Biol.
2006. 57:79–107

The *Annual Review of Plant Biology* is online at plant.annualreviews.org

doi: 10.1146/annurev.arplant.57.032905.105239

1543-5008/06/0602-0079$20.00

Key Words

confocal scanning laser microscopy, green fluorescent protein, biosensors, cameleon, live-cell imaging

Abstract

A substantial number of elegant experimental approaches have been developed to image the distribution and dynamics of DNA, mRNA, proteins, organelles, metabolites, and ions in living plant cells. Although the human brain can rapidly assimilate visual information, particularly when presented as animations and movies, it is much more challenging to condense the phenomenal amount of data present in three-, four-, or even five-dimensional images into statistically useful measurements. This review explores a range of in vivo fluorescence imaging applications in plants, with particular emphasis on where quantitative techniques are beginning to emerge.

Contents

INTRODUCTION

The widespread use of intrinsically fluorescent proteins (IFPs) and greater availability of advanced microscope systems have dramatically increased routine use of microscopy in plant research. This review focuses on live-cell imaging techniques, with emphasis on where the discipline is shifting from qualitative to quantitative analysis. Quantitative analyses require significantly more rigor in experimental design and methodology than comparable qualitative assessments, but are of increasing importance if results are to be compared statistically and meaningfully between different laboratories, and are essential to develop mathematical simulations of the underlying processes. This has a direct bearing on the extent it will be possible to integrate imaging information efficiently within systems biology.

LIFE IN THE NUCLEUS

The plant nucleus can be irregular, with extensive convoluted grooves and invaginations (19), and can become distorted during rapid movement, particularly in root hairs (18, 132). However, within the nucleus, evidence from fixed tissues suggests chromosomes and key processes such as replication, transcription, and mRNA processing are spatially organized (77). Recently, tools were developed to visualize the dynamics of these processes. Thus, discrete regions of chromosomes can be tagged by inserting a concatenated target sequence, such as the *lac* operator, and visualized following binding of green fluorescent protein (GFP) fused to the appropriate DNA-binding domain (LacI) (62) (**Figure 1*a***). Quantifying fluorescent spot number and amount of DNA from DAPI staining provides information on the level of endoreduplication and the degree of chromatid coherence (62, 63). The intranuclear chromatin diffusion coefficient (D) can be quantified from the spot dynamics, whereas movement relative to other loci describes the local confinement volume within each chromosome territory. These measures vary between different cell types. Thus D was ~twofold lower in epidermal versus stomatal guard cells, whereas the confinement volume was sixfold greater (63). The origin of these differences is not known, but may reflect epigenetic mechanisms influencing differential gene expression in the two cell types (63) or even biophysical effects of different turgor pressure. Although tagged loci provide new insights into intranuclear dynamics, they have drawbacks. Whereas chromosome painting using fluorescence in situ hybridization (FISH) shows that most chromosomes are randomly distributed, with slight preferential association of chromosomes carrying nucleolar organizer regions (NORs) (106), tagged loci have a higher than expected association with each other and with endogenous heterochromatin (105). Despite this caveat, in vivo tagging would be useful to test predictions from simulation models based on D and the rate of directed telomere movement during "bouquet" formation in meiotic cells (15).

Intranuclear dynamics have also been observed for GFP-tagged splicing factors. During transcription, splicing factors are recruited to spliceosomes from storage sites (interchromatin granule clusters) that appear as speckles in the nucleus. The number of speckles varies between different cell types, and their intensity varies inversely with transcriptional activity (29, 32). Speckles appear to move within a constrained volume, but can also bud, fuse, assemble, and disassemble (29, 32). Movement is abolished by blocking transcription and cannot arise simply from diffusion (32). An increasing number of proteins not directly involved in mRNA processing also cluster in intranuclear speckles (82, 94, 144), but the functional significance of this localization is not known.

QUANTITATIVE IMAGING OF GENE EXPRESSION

Recent advances in genomic technologies have enabled simultaneous measurement of thousands of gene expression profiles with increasing quantitative precision from progressively smaller tissue samples (89). However, there is often little correlation between levels of mRNA and expressed protein, necessitating parallel high-throughput proteome analysis, which currently requires much larger tissue samples. Conversely, when expression has been monitored for individual cells in a notionally homogeneous population, considerable variation in expression capacity (19a), and an extraordinary range of expression profiles have been reported, encapsulated as "the myth of the average cell" (79). Increased spatial resolution is possible with laser micro-dissection of single cells or micro-sampling (89), or by imaging following in situ hybridization or in situ polymerase chain reaction (107), but these techniques are difficult to convert to a high-throughput format suitable for time-resolved analysis of different cell types during development or in response to environmental stimuli.

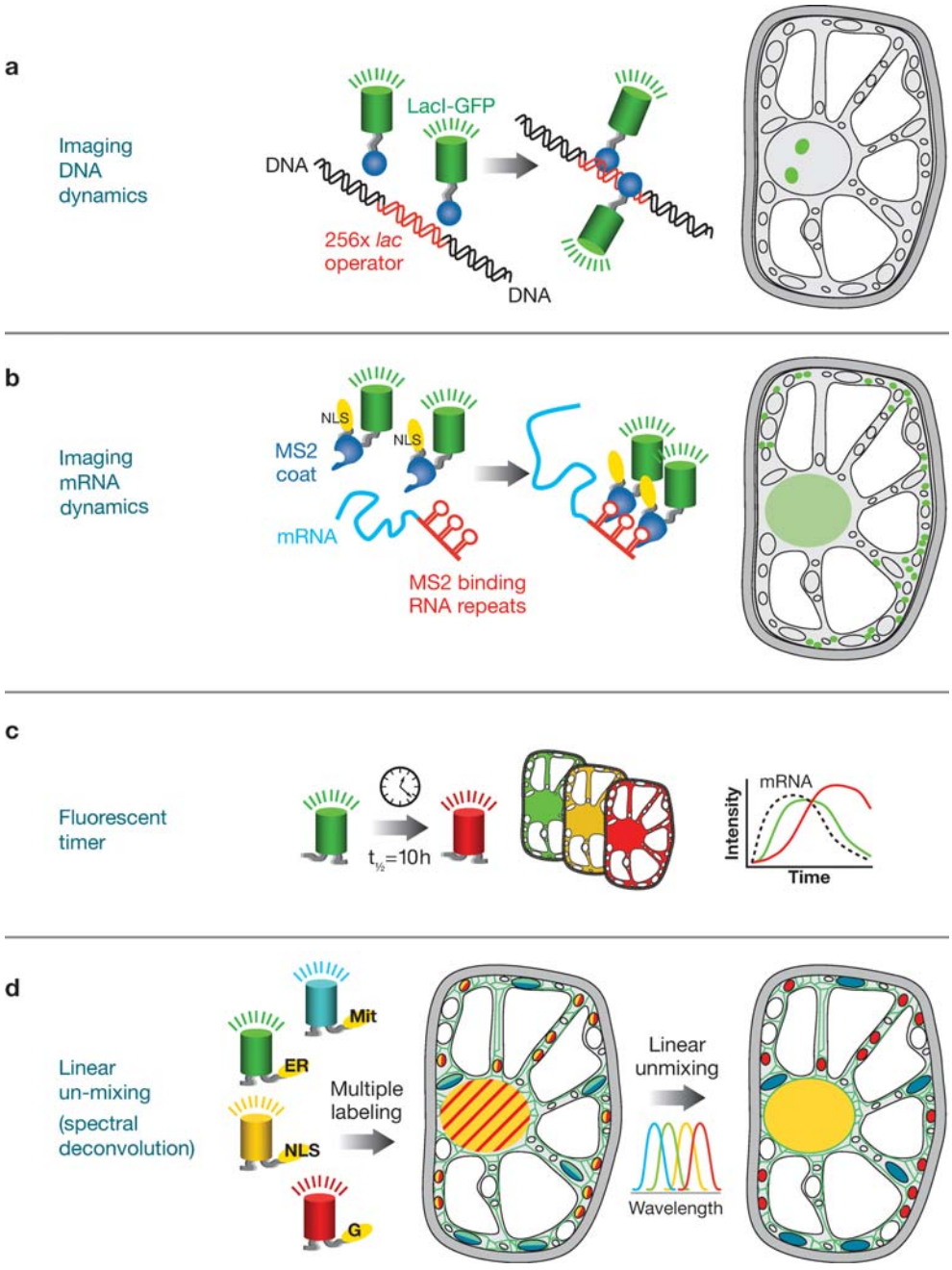

Figure 1

Schematic representations of the quantitative imaging techniques described in this review. Fluorescent proteins (*cylinders*) are color coded to represent their characteristic emission peak and the relative levels of emission are shown by the lines above. Targeting sequences are shown in yellow. High-intensity laser illumination is indicated by lightening symbols and normal excitation by wavy arrows. The clock symbol represents a passage of time. NLS, nuclear localization sequence; ER, endoplasmic reticulum; G, Golgi; Mit, mitochondria.

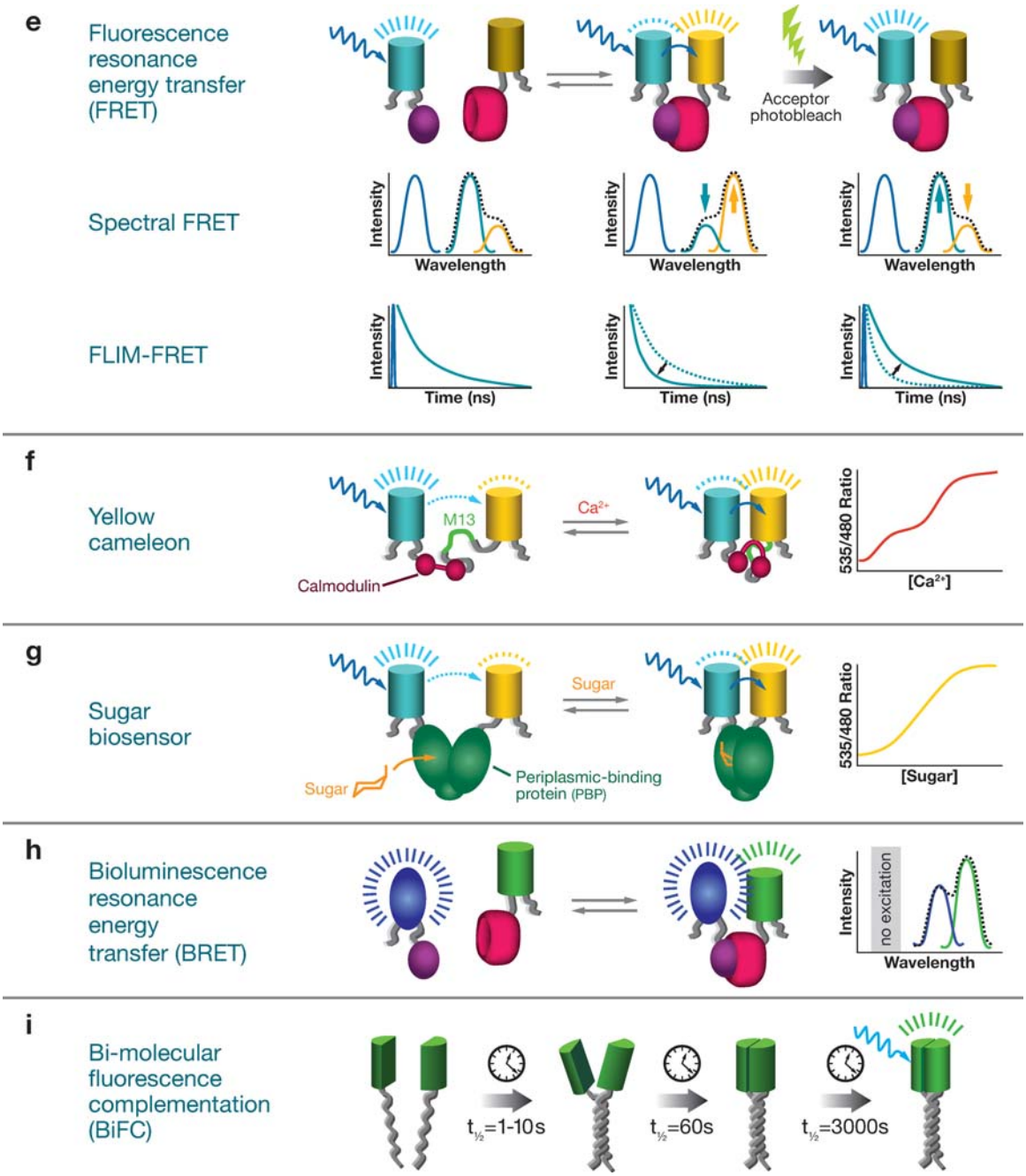

Figure 1

(*Continued*)

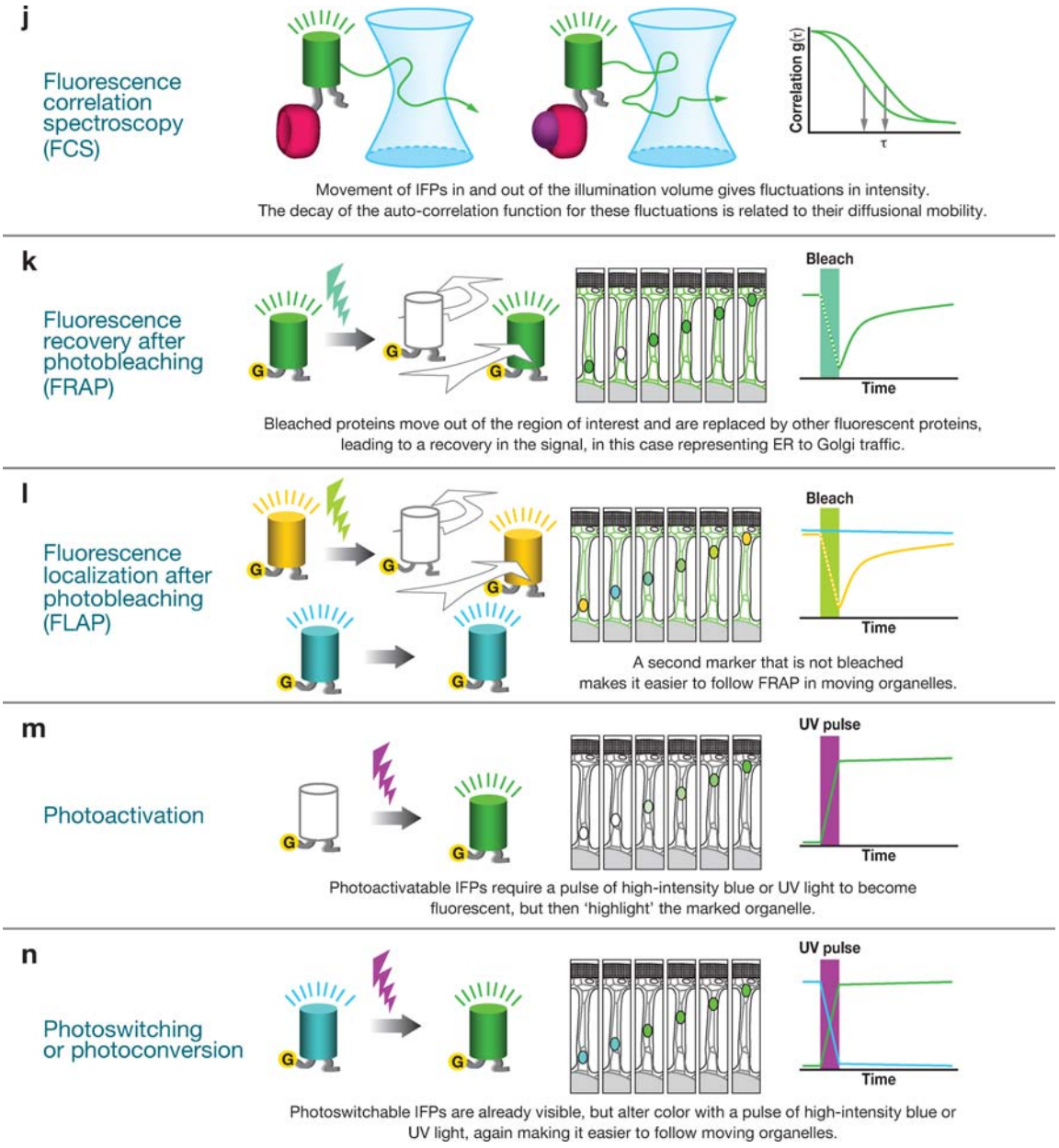

Figure 1

(*Continued*)

In Vivo Imaging of mRNA Localization and Dynamics

Recently, tools were developed to follow mRNA dynamics by adding a stem-loop aptamer sequence to the mRNA that is recognized by a coexpressed fluorescently tagged partner (10). For example, a GFP fusion with the bacteriophage MS2 coat protein can be used to visualize concatenated repeats of the 19-base pair (bp) MS2-binding

RNA sequence (**Figure 1*b***). This confirmed that specific mRNA molecules are localized to endoplasmic reticulum (ER) subdomains and revealed that tagged-RNA particle movement is actin based (50). In situ hybridization shows that other specific transcripts are also spatially localized (100), and in *Acetabularia*, 6 out of 12 mRNAs examined showed cytoskeleton-dependent asymmetric distribution (135), suggesting mRNA localization may be widespread. The aptamer-partner system might allow more systematic investigation of this phenomenon. The tagging approach is also useful for plant viruses that do not tolerate insertion of additional reporter sequences (147), and may even be adaptable to track non-cell-autonomous movement of small RNA molecules (146).

In Vivo Imaging of Promoter Activity

Promoter-GFP constructs are widely used to monitor promoter activity from individual cells to plants under field conditions (48), although quantitation in vivo may require correction for light absorption by endogenous plant pigments (149). Even with notionally constitutive promoters, a mosaic pattern of expression can occur (7), and reproducible expression may require matrix attachment regions (MARs) flanking the promoter-GFP (49) or mutants defective in post-transcriptional gene silencing (14a) to reduce local gene silencing events.

Unmodified GFP is less useful to quantify transient expression as the fluorescent signal reflects both promoter activity and fluorophore maturation, which gives a lag before fluorescence is detectable. Likewise, the stability of GFP ($t_{1/2} > 24$ h) obscures any reduction in promoter activity. Promoter-luciferase constructs are regarded as better reporters for transient expression as the light output more closely matches the level and timing of mRNA changes (45, 144a). More rapid GFP turnover can be achieved by adding protein- or mRNA-destabilizing elements that reduce the half life to ~3 h (136). Such approaches have been used for luciferase and β-glucuronidase in plants (143), but have not yet been applied to GFP.

An alternative method to analyze transient gene expression uses the DsRed "timer" fluorescent protein that slowly matures from a green to a red fluorescent form, distinguishing changes in gene expression by color (91, 129). Thus, immediately following gene induction, the signal is exclusively green, steady-state expression gives a defined G/R ratio (depending on the precise imaging configuration), and a decrease in expression shifts the ratio increasingly toward the red (**Figure 1*c***).

PROTEIN LOCATION, LEVEL, AND TURNOVER

Fluorescent-Protein Fusions

In-frame fusions with IFPs are straightforward to generate, compared to immunoprobes, and greatly facilitate visualization of intracellular protein distribution and dynamics. Ideal IFP tags should be nondimerizing monomers without any targeting motifs that fold efficiently and can tolerate N- or C-terminal fusions. They should have high molar extinction coefficients, quantum efficiency, and photostability that are insensitive to the local environment. Suitable monomeric IFPs spanning the entire visible spectrum have been isolated from different species, or generated by ingenious rational design and molecular evolution (131).

Tagging Traumas

IFP fusions have provided significant insights into a number of developmental and physiological processes, including subcellular organization of metabolic pathways into metabolons (1, 41), dissection of non-cell autonomous protein (NCAP) movement through the phloem (123), movement of transcription factors in meristems (96), or screening localization of unknown proteins (31). Despite the power of this approach, it is

important to validate that the pattern observed for the fusion protein reflects the true behavior of the native target. There is high confidence if the fusion protein, driven from its own promoter, complements a null mutant and the distribution pattern is confirmed by alternative techniques, such as immunocytochemistry (96). These stringent criteria have become an almost *de facto* requirement in tractable genetic organisms, such as yeast. In the next few years they will become the accepted standard in plants. In contrast, tagging with the IFP and driving expression of the fusion protein from a strong promoter can generate artifacts ranging from protein aggregation, steric interference in targeting or complex formation, saturation of normal transport and targeting pathways, and generation of phenotypes resulting from overexpression of the protein. Even when targeting is not impaired, IFP tagging can generate dominant inhibitory alleles, particularly when the tagged protein is involved in protei-protein interactions.

For example, Actin can be visualized in vivo by binding of GFP-mTalin (70). However, labeling has a major impact on actin organization (65). GFP-Fimbrin is less disruptive (120), but high levels of expression still give stunted phenotypes (138) and disrupt organelle dynamics (J. Runions, unpublished data). Rab GTPases can be localized as IFP fusions (71, 121a, 131b), but some IFP tags generate a dominant-negative phenotype with similar sorting defects as untagged dominant-negative point mutants (71). In assays of subcellular targeting or transport, it is important that the IFP tag has no intrinsic sorting information. This is not always the case and the effect is species and cell-type dependent. Thus, in tobacco epidermis, a secreted mRFP1 marker is transported exclusively along the default secretory pathway and an equivalent GFP marker also appears in the vacuole, suggesting GFP contains a weak vacuolar sorting determinant (148), similar to the situation in yeast. Conversely, in tobacco BY2 suspension culture cells, mRFP1 also accumulates in vacuoles (145). In other cases, overexpression of IFP-tagged proteins, such as the vacuolar sorting receptor BP80, appears to compete with endogenous receptors, causing sorting defects (22).

More subtle errors can arise from the different properties of each IFP. For example, EYFP (pK_a 7.0) is more sensitive to quenching in acidic compartments than other IFPs, making them less obvious when labeled with EYFP compared to an identical GFP construct (148). This could lead to significant misinterpretation of the intracellular distribution of certain fusion proteins. On the positive side, the pH sensitivity of YFP can be used to infer whether particular protein loops or termini are cytoplasmic or extracellular (127). Although GFP fluorescence is less sensitive to pH, blue-light-dependent conformational changes in GFP make it a target for degradation by vacuolar proteinases at acidic pH, leading to a loss in signal in tissues exposed to the light (128). Whether comparable light-dependent degradation occurs for other IFPs is not yet known.

Protein Concentration Controls

Almost no reports attempt to calibrate IFP expression levels against appropriate standards, but rely on subjective comparisons of relative expression levels ("dim" or "bright"). A notable exception is the recent work in yeast that combined quantitative imaging of YFP-fusion proteins, driven from their endogenous promoters, with either quantitative immunoblotting or flow cytometric analysis (143a). Of greater concern is the absence of proper reference images to relate the apparent expression level to the amount of protein in different cell types. For example, the visual impression of uniform gene expression is deceptive and skewed to regions with higher net cytoplasmic density (meristems, vascular tissue, and stomatal guard cells). Protein concentration controls are routinely used when running gels and we advocate equivalent controls should be used when imaging tissues (e.g., 37).

Low-Molecular Weight Genetically Encoded Tags

A variety of much smaller fluorescent tags have been developed to label proteins in vivo that circumvent potential steric interference associated with IFP fusions (61). Thus, the small tetra-cysteine peptide motif (Cys-Cys-Pro-Gly-Cys-Cys) binds fluorescent bis-arsenical ligands with high affinity ($\sim 10^{-11}$ M) to give a fluorescent complex (47). Three fluorescent ligands, with different spectra based on xanthene (CHoXAsH), fluorescein (FlAsH), or resorufin (ReAsH), are now commercially available (Invitrogen, Lumio™ series). The ligands are applied as membrane-permeant complexes with 1,2-ethanedithiol (EDT). Once in the cell, the tetracysteine hairpin displaces the EDT to generate a minimally disrupted fluorescent fusion protein. As an example, a tubulin-TetCys fusion rescues yeast cells lacking tubulin, whereas GFP-tubulin is unable to functionally complement the mutant (5).

Under high levels of illumination, these fluorophores produce singlet oxygen capable of inactivating proteins in the immediate vicinity, in a process termed chromophore-assisted light inactivation (CALI) (130). This could provide a novel means to knockdown specific tagged proteins with a high degree of spatial and temporal resolution.

Multichannel Imaging in Plants

The range of IFPs available has dramatically increased possibilities for multiple labeling and colocalization analysis in vivo (64). To provide unambiguous results, it is essential that the signals from the different spectral variants can be unequivocally isolated, either through minimizing bleed-through between different channels (64) or by spectral deconvolution (linear unmixing). Bleed-through can be reduced by rapid switching between different excitation/emission combinations at millisecond intervals to avoid movement artifacts. Although enhanced GFP is brighter and excited efficiently at 488 nm, the spectral properties of the Haseloff mGFP5 variant are better suited to separate GFP and yellow fluorescent protein (YFP) using line switching with 458/514-nm excitation.

Spectral Imaging and Linear Unmixing

A number of imaging systems now implement simultaneous or sequential collection of several spectrally distinct channels to give a stack of wavelength (lambda, λ) images (150). Even if fluorophores (or autofluorescence) have a high degree of spectral overlap, their individual contributions can be extracted by linear unmixing of the spectrum recorded at each pixel using appropriate reference spectra (9, 150) (see **Figures 1*d***; **2*a*,*b***). Protocols have been developed to optimize the number of channels and their bandwidth needed to separate particular fluorophores (98). Linear unmixing is only possible if signals from the individual channels are within the dynamic range of the instrument. This can be difficult to achieve, particularly in multiple-construct transient expression systems. Using the FMDV 2A peptide (48a) or internal ribosome entry sites (IRES) (144a) to generate stoichiometric quantities of two polypeptides from a single transcript may be advantageous in this respect (**Figure 2*c–e***).

Quantitative Colocalization Analysis

Colocalization describes the extent that two (or more) probes occur at the same physical location in the cell. Before colocalization can be quantified, it is essential that spectral bleed-through is eliminated, pinholes are aligned, and images are properly registered and not affected by chromatic aberration (142). Threshold values are chosen to remove background, ideally using objective criteria (20). Pearson's coefficient or the overlap coefficient provide a single measure of colocalization. However, it is more informative to analyze the proportion of each probe contributing to the colocalized pixels as separate coefficients (81). Even with

confocal and multiphoton systems, the blurring associated with the point spread function (psf) can give erroneous superposition of adjacent objects and intermediate values of colocalization. De-convolution of the three-dimensional (3D) image prior to colocalization analysis reduces these artifacts and improves quantitation (78). Furthermore, the significance of the coefficients can be assessed by comparison with an expected random

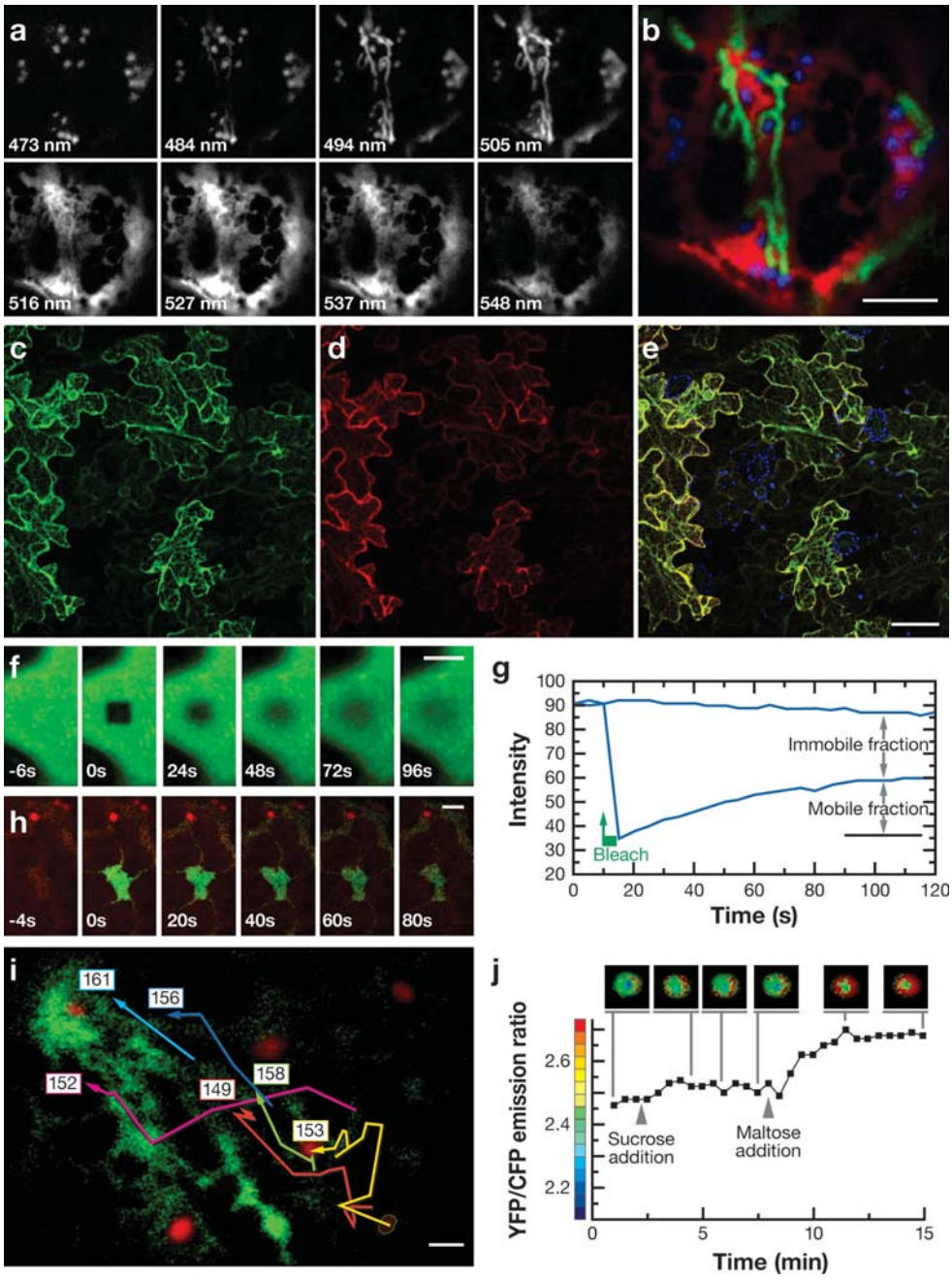

pattern obtained by repeatedly randomizing the pixel distribution in one of the channels (20). Despite the availability of appropriate software and the widespread use of multiple labeling experiments purporting to assess colocalization, quantitative analysis (1) is still rare in plant systems.

PROTEIN-PROTEIN INTERACTIONS

Although colocalization is a prerequisite for two molecular species to interact, it cannot readily be used to demonstrate that physical association has occurred. Fortunately, a number of other live-cell techniques, such as fluorescence (or Förster) resonance energy transfer (FRET), bioluminescence resonance energy transfer (BRET), fluorescence correlation spectroscopy (FCS), or bi-molecular fluorescence complementation (BiFC), can provide this information.

Fluorescence Resonance Energy Transfer

FRET describes the radiationless transfer of energy from a donor fluorophore to an adjacent acceptor fluorophore that has significant spectral overlap and appropriate orientation

Figure 2

Quantitative imaging of protein levels and dynamic processes in plants. (*a*, *b*) Linear unmixing of signals from cyan fluorescent protein (CFP), green fluorescent protein (GFP), and yellow fluorescent protein (YFP). Spectral images in 10.7-nm bands centered on the wavelengths indicated (*a*) were collected using the Zeiss LSM510 META detector system from epidermal cells of the lower epidermis of *Nicotiana tabacum* four days after infiltration with three different *Agrobacterium* strains containing plasmids that express ST-ECFP, to label Golgi, GFP targeted to mitochondria, and YFP-HDEL to label the ER. The considerable spectral overlap between the signals from each organelle was resolved using linear unmixing with reference spectra collected under identical conditions (*b*). Scale bar = 5 μm. (*c–e*) Stoichiometric expression of GFP and YFP using the FMDV 2A peptide. Images were collected from epidermal cells of the lower epidermis of *Nicotiana tabacum* four days after infiltration with *Agrobacterium* containing a single construct expressing cytoplasmic YFP and endoplasmic reticulum (ER)-targeted mGFP5 linked by the FMDV 2A peptide. Cleavage between the IFPs released two separate fluorescent proteins and the signals were separated by rapid line switching between ex 458 nm, em 475–525 nm (*c*), and ex 514 nm, em 535–590 nm (*d*). Autofluorescence from chloroplasts was imaged at >650 nm (coded in *blue*). At low inoculum densities, there is considerable variation in expression between different cells in the epidermis, yet the ratio of the two fluorescent proteins remains almost constant in the merged image (*e*) (M. Samalova & I. Moore, unpublished data). (*f, g*) Measurement of plasma membrane protein mobility using fluorescence recovery after photobleaching (FRAP). LTI6B-GFP marks the plasma membrane of *Arabidopsis* leaf epidermal cells, shown here as a single paradermal optical section (*f*). A high-intensity laser pulse was used to bleach a rectangular region at t = 0 s. Movement of fluorescent protein from adjacent areas gave a recovery in signal over time (*f, g*) that was analyzed to give the fraction of mobile molecules and the half time for recovery ($t_{1/2}$ 27.9s) (J. Runions, unpublished data). Scale bar = 20 μm. (*h*) Measurement of ER protein mobility using photoactivatable GFP (PAGFP). Calnexin-was PAGFP localized to the ER membrane (weakly labeled in *red* with a second marker), but gave very little fluorescence with excitation at 488 nm until it was activated with a high-intensity pulse of short wavelength light (405 nm) at t = 0 s. The highly localized increase in fluorescence subsequently dissipated as the calnexin dispersed through the ER (112). Scale bar = 2 μm. (*i*) Tracking movement of Golgi bodies in leaf epidermal cells of *Nicotiana*. Golgi bodies (*red*) were imaged in confocal time series and automated tracking software was used to measure their movement patterns (*numbered*, *colored lines*). The ER membrane was highlighted with photoactivated GFP (*green*) (112). Scale bar = 1 μm. (*j*) Measurement of maltose uptake in yeast using a fluorescence resonance energy transfer (FRET)-based sensor. Intracellular maltose concentrations were imaged with a genetically encoded sensor that incorporated a hinged maltose-binding element between CFP and YFP. Uptake of maltose, but not sucrose, into the cytoplasm resulted in a conformational change in the hinged segment and an increase in FRET, measured as a change in the YFP/CFP emission ratio. The pseudo color-coded images show the relative increase in the YFP/CFP ratio. Adapted from Reference 33 with permission.

(**Figure 1*e***). FRET efficiency falls off with the inverse sixth power of the fluorophore separation. The distance at which energy transfer is reduced by 50% (the Förster radius) is around 3–6 nM for common donor-acceptor pairs (39, 55). FRET can be detected spectrally as a decrease (quenching) of donor emission with commensurate increase in sensitized acceptor emission, or as a decrease in the fluorescence lifetime (τ) of the donor fluorophor, measured using fluorescence lifetime imaging microscopy (FLIM). Quantitative measurements, particularly of steady-state protein association, need controls to accommodate background, auto-fluorescence, bleed-through, photobleaching, and different environmental sensitivity of the fluorophores (39, 55). FLIM-FRET can be determined just from the donor fluorescence lifetime (58), although the extent of protein-protein interaction still depends on the stoichiometry of the interacting partners. The most common, but irreversible, control to validate that FRET really occurs is to bleach the acceptor and measure the resulting increase in donor fluorescence intensity or lifetime.

The range of molecular interactions probed by FRET is increasing slowly and includes dimerization of transcription factors (58, 64) or receptors (113, 116), formation of lipid domains (134), interactions between subunits in a single functional protein complex (66) or "metabolons" (1), complexes of plastid division proteins (81a), and association of regulatory or signaling proteins (8, 11, 82, 117). One of the biggest problems in FRET measurements is reproducible control of tagged-protein stoichiometry, which may also benefit from application of the FMDV 2A peptide (48a) or IRES (144a) technology. In some cases it may be advantageous to use a luminescent donor, such as luciferase, and BRET (125, 126) (**Figure 1*b***). BRET avoids problems with autofluorescence, photobleaching, direct acceptor excitation, or triggering light-dependent signaling pathways, but has lower spatial resolution than FRET.

Fluorescence Correlation Spectroscopy

FCS provides an alternative means to characterize fluorophore mobility, concentration, and interaction in vivo (114). FCS works by measuring the time series of fluctuations in signal as fluorescent molecules move in and out of a small excitation volume, typically achieved with stationary confocal or multiphoton optics (**Figure 1*j***). The decrease in the autocorrelation function of the time series provides a measure of the diffusion coefficient of the fluorophore. Thus, the cytoplasmic concentration of GFP driven from a 35S promoter was measured as 0.1-1 μM and the cytoplasmic diffusion coefficient as $4 \pm 2 \times 10^{-7}$ cm^2 s^{-1} (69). Diffusion of single GFP molecules and larger aggregates were quantified in chloroplast stromules, with some evidence of active transport, possibly along a "plastoskeleton" (69). FCS has also been used to measure the location, accumulation, and mobility of fluorescently tagged Nod factors in membranes and the cell wall from very low-bulk concentrations (42). Although complex formation does affect the diffusion coefficient measured by FCS, fluorescence cross-correlation spectroscopy (FCCS) between two fluorescently tagged species provides a more sensitive measure of protein-protein interaction (68).

Bi-Molecular Fluorescence Complementation

BiFC may provide a simpler test for protein interaction in vivo. Potential interacting partners are tethered to specific nonfluorescent fragments of IFPs. If the partners bind, the fragments associate to form a bi-molecular complex capable of reconstituting fluorescence (**Figure 1*i***). Complex formation is essentially irreversible, which prevents imaging of changes in protein association state, but captures weak or transiently interacting partners. Very high levels of expression of the IFP fragments can yield nonspecific interaction (137), and not all permutations of C or N

tagging are effective (13), probably because of steric constraints on the interacting partners. In plants, BiFC has been used to assess homo- or heterodimerization of transcription factors (27, 137), chromodomain proteins (13), 14-3-3 proteins (137), complex formation between plastid division proteins (81a), and the α and β subunits of protein farnesyltransferase (13). Other BiFC strategies use reconstitution of fragments from murine dihydrofolate reductase (mDHFR) that bind a fluorescein-conjugated inhibitor, methotrexate, with high affinity (124). The authors followed decreases as well as increases in fluorescence (124). This implies that mDHFR complex formation is reversible or turns over on a timescale of hours, unlike BiFC with IFPs. If this is a general feature of the mDHFR system it may provide a dynamic readout of protein-protein interactions rather than just a cumulative response.

MEASURING PROTEIN AND ORGANELLE DYNAMICS

Quantitation of Organelle Motility

There is a long history in microscopical measurements of organelle motility using phase and Nomarski imaging. Fluorescent labeling of organelles provides greater contrast that facilitates quantitative tracking of various organelles including nuclei (132), Golgi bodies (97, 112, 145), peroxisomes (83), and microtubules (26, 119). Although much plant work has used manual tracking from 2D time-lapse images, several algorithms have been developed for (semi-)automated tracking in 4D (40). For example, Runions et al. (112) tracked hundreds of mRFP-tagged Golgi bodies to determine their average velocity and track profile characteristics (**Figure 2*i***).

Measurement of Protein Dynamics Using Photobleaching or Photoactivation

During time-lapse imaging, fluorophore in a defined region of interest (ROI) can be bleached by high-intensity illumination. Fluorescence recovery after photobleaching (FRAP) occurs as unbleached fluorophore moves back into the bleached area (**Figure 1*k***) and provides a measure of the rate of movement and the underlying movement mechanism (122). If the goal is to determine total connectivity within an extended membrane system, such as the ER, continuous bleaching of the ROI will eventually drain signal from all connected compartments (139), termed fluorescence loss in photobleaching (FLIP).

FRAP is useful at various levels from exchange between cells or organelles (75, 139), diffusion of proteins within membranes (**Figure 2*f*,*g***) or organelles (112, 139), down to protein turnover in complexes (32). For example, Hush et al. (57) first employed FRAP in plants using carboxyfluorescein-labeled tubulin to study microtubule dynamics. Subsequently, FRAP revealed microtubule translocation through treadmilling in cortical arrays (119) and dynamic interactions with microtubule-associated proteins (MAPs) (16). Whereas FRAP or FLIP are straightforward between fairly static structures, such as chloroplasts connected by stromules (75), it is technically more difficult if the target protein or organelle is moving, not least because it becomes invisible immediately after the bleach. To aid in localization post-bleach, a second fluorophore can be introduced to the target that remains visible throughout the time course (14, 21, 139), termed fluorescence localization after photobleaching (FLAP) (**Figure 1*l***).

Photoactivation

As an alternative strategy, Patterson & Lippincott-Schwartz (104) developed photoactivatable (PA) GFP to fluorescently highlight proteins in targeted subcellular regions or organelles. PA-GFP shows a 100-fold increase in fluorescence after a brief pulse of irradiation with near UV (104) (**Figure 1*m***). PA-GFP works in plants and has been

targetted to Golgi bodies and peroxisomes and used to follow ER dynamics (112) (**Figure 2*b***). Recently, the first photoactivatable red fluorescent protein (PA-mRFP1-1) was developed (133), although it currently has a relatively low extinction coefficient and quantum efficiency, and requires prolonged UV exposure for activation.

Photoactivation has the converse problem to FRAP. The absence of signal prior to irradiation that makes it difficult to find cells or organelles expressing PA-GFP. One solution is to use double labeling, similar to FLAP. An alternative strategy is to use IFPs that are fluorescent initially, but shift color upon intense illumination (photoswitching or photoconversion) (**Figure 1*n***). This provides a reference image of the entire labeled structure, while following the dynamics of a selected portion. For example, Kaede gives a 200-fold increase in green-to-red emission following photoconversion with (ultra-)violet illumination. As the native Kaede protein is a tetramer, it is not appropriate as a fusion tag, but may be used for organelle tracking (4) and has been used to probe transient fusion and fission events of mitochondria (6). More recently, several monomeric photoswitchable fluorescent proteins suitable for tagging were developed, including photoswitchable cyan fluorescent protein (PS-CFP) that gives a 1,500-fold increase in green-to-cyan fluorescence following (ultra-)violet excitation (17) and EosFP (142a) and KikGR (131a), which both shift from green-to-red fluorescence with (ultra-)violet irradiation. Although there are no full papers reporting the use of these photoswitchable proteins in plants, preliminary data indicate they are expressed in a functional form and can be photoconverted effectively (16a).

Under low O_2 levels, S65T GFP from *Aequori victoria* can be converted to a red fluorescing form with high-intensity illumination at normal excitation wavelengths, and has been used to show luminal continuity of mitochondria in anaerobic *Saccharomyces cerevisiae* (60). This technique may even be useful to assess onset of anoxia for any GFP-labeled specimen on the microscope.

QUANTITATIVE MORPHOLOGY AND DEVELOPMENTAL STUDIES

Three-Dimensional Measurement of Cell and Organelle Size

Confocal, multiphoton, or wide-field deconvolution imaging can all sample 3D volumes, facilitating quantitative analysis of morphology (**Figure 3*a*,*b***). Volume measurements using intensity-based segmentation require correction for depth-dependent signal attenuation and z-axis distortion (36, 44, 121, 142) (**Figure 3*c–f***) and are sensitive to the segmentation threshold used. Surface-area measurements also depend on the "granularity" of the voxel dimensions and sampling noise. 3D segmentation using deformable meshes that grow to fill cell volumes are reported to give more robust results that are less sensitive to noise (52).

An alternative approach is to use stereology to quantify geometrical properties (number, length, surface area, or volume) by counting interactions with randomly positioned sampling probes. Points probes are used to measure volumes, lines to measure surface areas, planes to measure lengths, and volumes to count numbers (56, 72). Stereological techniques work particularly well for volume measurements from confocal datasets (72, 86, 88) (**Figure 3*g–j***).

Even when cellular objects approach the 3D dimensions of the point-spread function (psf), their "true" volume can be estimated using 3D model-based approaches that incorporate a measured psf (12). Meckel et al. (84) used a simplifying 2D (x,y) Gaussian model to analyze populations of vesicles in guard cells, on the assumption that these objects are spherical.

Quantitation of Morphology and Lineage at the Tissue Level

Confocal z-series of fixed and cleared specimens are useful to study patterns of cell division and elongation during development (52) (**Figure 3*a*,*b***). Recently, techniques for 4D in vivo confocal imaging of the surface layers of intact meristems were developed using combinations of FM dyes, IFP markers, and spectral unmixing (43, 52a, 110, 110a). 3D and 4D imaging of larger intact structures is also possible using optical coherence microscopy (OCM) (54, 111) or optical projection tomography (OPT) (118; E. Coen & K. Lee, personal communication). OCM is an interference technique based on back-scattered light, whereas OPT can be used in either transmission or fluorescence mode (118). In theory, OPT could be used with the many fluorescent lineage markers available, including those developed for constitutive or inducible transgene activation. Relatively precise spatial and temporal cell marking is also possible through local heat activation by repeated laser scanning of a heat-shock promoter that drives expression of Ac transposase. This removes a DS1 element inserted between the 35S promoter and H2B-YFP, which then marks nuclei in the targeted cells and the lineage of their progeny (74) (**Figure 3*k***).

IMAGING IONS AND METABOLITES

Genetically Encoded Ca^{2+} Sensors

Tsien and colleagues pioneered construction of genetically encoded ion sensors using FRET with the development of the cameleon probes for Ca^{2+} (93). FRET probes retain the highly desirable ratioable properties of the best chemical Ca^{2+} dyes, but are introduced by transformation rather than potentially damaging microinjection. They are relatively photostable, nontoxic, and are not sequestered by cellular detoxification systems. Furthermore, their sensitivity can be adjusted by modifying the ligand-binding sequence and they can be targeted to different subcellular compartments.

In the yellow cameleons, CFP and YFP are linked by calmodulin (CaM) and the M13-CaM-binding peptide from myosin light-chain kinase (**Figure 1*f***). On binding Ca^{2+}, the CaM alters its conformation, binds to M13, and brings the fluorophores together with an increase in FRET (93). Most confocal systems do not have an appropriate blue (432-nm) excitation source. However, it may be possible to use the common Ar-ion 458-nm line and recover changes in FRET by spectral unmixing (59).

YC2 has a biphasic Ca^{2+} response with K'_d values of 70 nM and 11 μM. The K'_d values do not vary with pH, Mg^{2+}, and ionic strength at physiological levels, probably as the CaM-based sensor is naturally tailored to operate in a cytoplasmic milieu. This should make cameleon measurements more accurate than ratiometric dyes (93). For comparison, K'_d values for Indo-1 and Fura-2 increase 2-4-fold in vivo in animal cells. The corresponding shifts in plants are less clear as reliable in vivo calibrations are difficult (109). Introducing mutations in the Ca^{2+}-binding domains give the YC3 series (E104Q), with a single K'_d (4.4 μM), or the YC4 series (E31Q), with a lower affinity K'_d (700 μM), which are suitable to measure Ca^{2+} in ER (93).

Set against these benefits, cameleon expression levels are low, perhaps a few micromolar, and the relative ratio change (RRC) for a full response is only ~1.6–1.8. Furthermore, EYFP is quenched by mild acidification (pK_a 6.9) and Cl^- ions (K'_d 110 mM), and the CaM-M13 linker may interact with endogenous CaM or CaM-binding proteins. The pH sensitivity has been reduced (pK_a 6.1) by introducing mutations in EYFP (V68L and Q69K) to give YC2.1, YC3.1, and YC4.1 (92), which are the only cameleons so far used in plants (3, 59, 140). The YC2.3, YC3.3, and YC4.3 series use Q69M YFP (citrine), which lowers the pK_a further to 5.7, removes the Cl^- sensitivity, and gives better folding (46). However, the

most significant recent breakthrough is inclusion of circularly permuted Venus-YFP, which increases the RRC by 600% by altering the dipole orientation between the CFP and YFP couple (95).

Cameleons in Plants

Allen et al. (3) first generated stable *Arabidopsis* plants expressing YC2.1 and measured Ca^{2+} dynamics in guard cells in response to

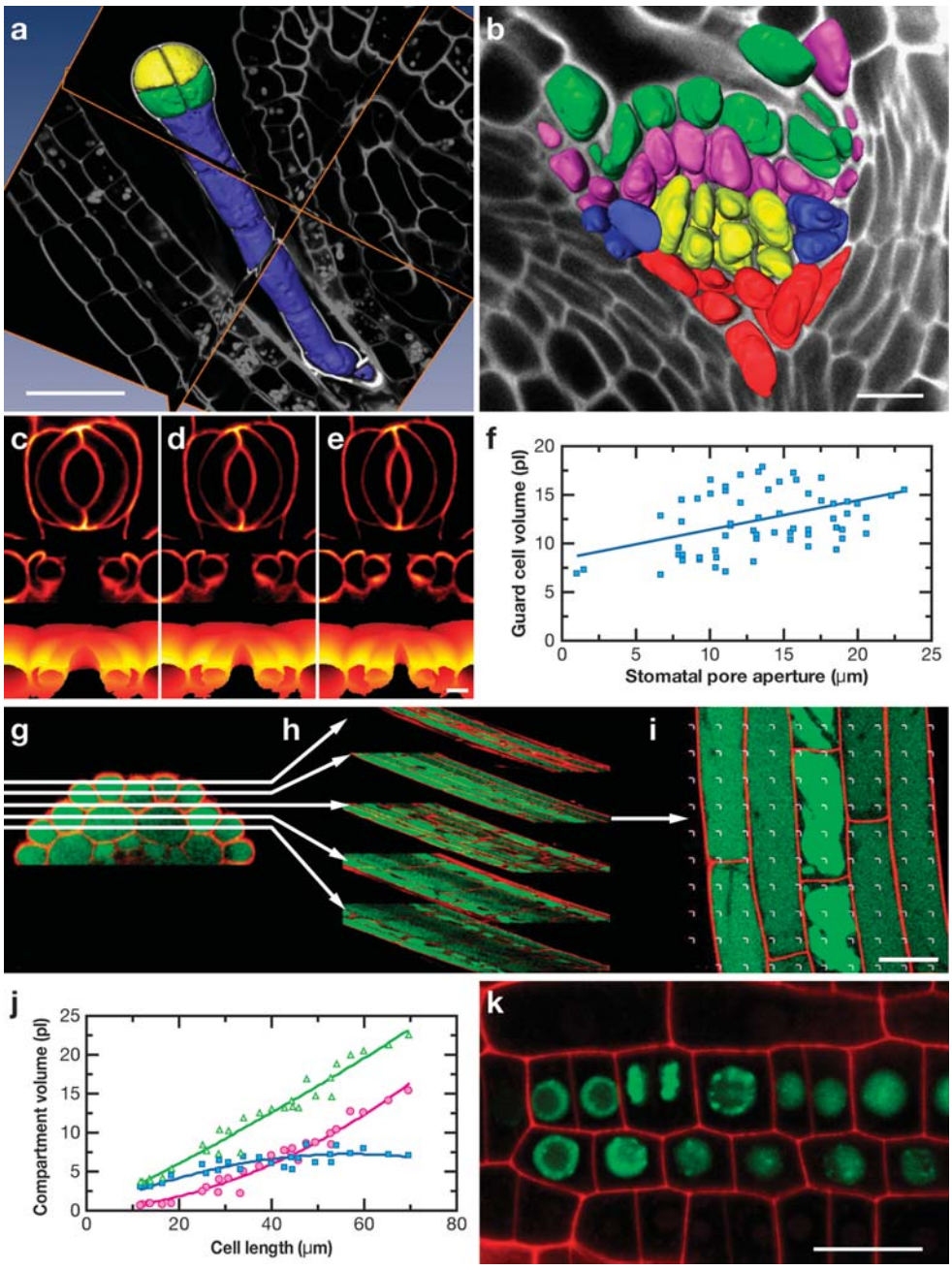

a range of stimuli and in different mutant backgrounds. YC2.1 has also been expressed in pollen tubes of *Lilium longiflorum* and *Nicotiana tabacum* (140), and YC3.1 in pollen tubes and stigmatic papillae of *Arabidopsis* (59). In general, results with the cameleons are comparable to previous reports with ratiometric probes. For example, cameleons report oscillating, tip-high Ca^{2+}-gradients in pollen tubes that are similar in magnitude to those reported with ratiometric dyes (e.g., 108). Likewise, localized repetitive transients were observed during pollen germination on stigmatic papillae (59), similar to those reported using microinjected Calcium Green-1 dextran (24). In stomatal guard cells, there is much more information on Ca^{2+} responses, and some interesting quantitative and qualitative differences, albeit derived from different species.

Comparison of Cameleon Measurements with Dye Measurements in Stomatal Guard Cells

Quantitatively, resting $[Ca^{2+}]_{cyt}$ in YC2.1-expressing *Arabidopsis* guard cells is 5–10-fold lower than that typically reported with ratiometric dyes. YC2.1 values may be more reliable because of the stability of the K'_d in cells and also because potentially disruptive iontophoretic microinjection is not needed. Qualitatively, all YC2.1 responses in wild-type *Arabidopsis* reveal transient spikes or oscillations, often with a delay following the stimulus and running on after the closing response has been triggered.

Interpretation of some YC2.1 results has been challenged (109), particularly those from experiments switching between hyperpolarizing (0.1 mM KCl) and depolarizing (100–mM

Figure 3

Quantitative imaging three-dimensional (3D) morphology in plants. (*a*, *b*) 3D reconstruction following intensity-based segmentation of confocal optical sections. High-contrast staining techniques were used to differentiate the cell wall from cell lumen, which were then filled and rendered to create a surface representation of cells and tissues. Cellular relationships were studied by rotating and slicing the reconstructions (J. Runions, unpublished data). (*a*) An eight-cell *Arabidopsis* embryo and suspensor within the ovule. Scale bar = 20 μm. (*b*) Vegetative shoot apical meristem of a mature *Arabidopsis* embryo. Scale bar = 20 μm. (*c–e*) 4D measurement of guard cell volume changes during ABA-induced stomatal closure. The cell wall in epidermal strips of *Commelina communis* was labeled with primulin and time-lapse 3D images collected with excitation at 442 nm. Images are presented as median (*x,y*) and (*x,z*) sections and as a height-coded projection, following correction for depth-dependent attenuation and intensity-based segmentation (142). The luminal volume was measured by seed filling the segmented volumes. Scale bar = 10 μ m. (*f*) Represents the relationship between guard cell lumenal volume and stomatal pore aperture (A. Parsons, M.D. Fricker & N.S. White, unpublished data). (*g–i*) Compartment volume measurements in *Arabidopsis* roots using stereological techniques. Stereology is a robust statistical method for morphological measurements and was used to determine changes in cytoplasmic and vacuolar volumes during elongation of trichoblasts in *Arabidopsis* roots using the Cavalieri estimator. 3D images were collected by two-photon laser-scanning microscopy following fluorescent labeling and vacuolar sequestration of glutathione (*green*) and cell walls with propidium iodide (*red*). (*g*, *h*) Uniform random sections (*h*) were overlaid with a point grid (*i*) and the cytoplasm, vacuole, and cell wall volumes were determined as a function of intersection with the grid (38, 86). Scale bar = 10 μm. (*j*) Shows the resultant relationship between cytoplasmic (*blue*), vacuolar (*red*), and total cell volume (*green*) for trichoblast cells in the elongation zone. (*k*) Light-activated lineage marking of cells in the *Arabidopsis* root epidermis. Local heating, generated by repeated laser scanning, was used to activate a heat-shock promoter driving expression of Ac transposase. The Ac transposase removed a Ds element from between the promoter and histone H2B-YFP gene allowing its expression (74). This change was heritable and marked nuclei of all cells derived from the initial event, enabling investigation of tissue origins and cell division patterns (*arrowhead*). Scale bar = 10 μm.

KCl) buffers to impose Ca^{2+}-oscillations (2). Plieth (109) generated almost identical ratio changes using this protocol in plants expressing either the Cl^--responsive Clomeleon indicator (73, 80) or the Ca^{2+}-indicator YC2.1. As Clomeleon does not contain the CaM-M13 Ca^{2+}-sensing linker, the implication is that some, if not all, of the YC2.1 response reflects changes in $[Cl^-]_{cyt}$ and pH, rather than $[Ca^{2+}]_{cyt}$. However, YC2.1 lacks the H148Q substitution used in Clomeleon, and only shows a slight shift in pK_a from 6.0 to 6.1 in the presence of Cl^- (46). Even a substantial drop in $[Cl^-]_{cyt}$ from ~150 mM to 0 mM, combined with cytoplasmic alkalinization from pH 7 to pH 8, would only give a 10–15% increase in YFP fluorescence in YC2.1 (46). As CFP is not affected, this would give a similar shift in the ratio value, irrespective of the prevailing $[Ca^{2+}]_{cyt}$. The magnitude of the Ca^{2+} spikes is much greater than these estimates, suggesting the potential for misinterpretation of these responses would be slight. Nevertheless, a Cl^- contribution to the lower plateau values might overestimate the level of apparent $[Ca^{2+}]_{cyt}$. Furthermore, the change in $[Cl^-]_{cyt}$ measured with Clomeleon (109) highlights the many other potential consequences of the Ca^{2+}-clamp protocol on guard cell physiology.

Why Are Oscillations Not Always Observed with Ratiometric Dyes?

In contrast to YC2.1, calcium responses measured with ratiometric dyes during stomatal closure have shown general increases of varying rate, magnitude, and duration, or occasionally no change at all, rather than just oscillations. This has a bearing on the current debate on whether information is encoded in the amplitude, frequency, or both of the Ca^{2+} signature or whether increases in $[Ca^{2+}]_{cyt}$ simply act as a chemical switch (53, 109, 115).

YC2.1 and ratiometric dyes differ in their intracellular concentration and rate of diffusion. The concentration of microinjected dye (<50 μM) is unlikely to buffer $[Ca^{2+}]_{cyt}$ directly. However, the rate of Ca^{2+}-dye diffusion may be sufficiently fast to dissipate localized Ca^{2+} gradients. In contrast, YC2.1, which diffuses more slowly, may report localized Ca^{2+} increases more faithfully. Messerli et al. (85) suggested a similar explanation for the higher estimated Ca^{2+}-gradient in pollen tubes measured with aequorin compared to ratiometric probes. There is some evidence for localized $[Ca^{2+}]$ elevations or waves using imaging (99), which might hint at spatial localization of the Ca^{2+} response. However, such measurements are prone to error and require careful masking of low-intensity signals, subtraction of both general background and structured auto-fluorescence, spatial and temporal filtering, and sufficiently high spatiotemporal resolution. Unfortunately, the areas that show the most interesting changes have the worst signal-to-noise, signal-to-background, and signal-to-auto-fluorescence ratios, and are the most prone to specimen and organelle movement artifacts and optical aberrations. This is a general problem in most plant cells in comparison with animal cells, as they tend to have a very thin layer of cytoplasm around the cell periphery and very active cytoplasmic movements.

The Spectre of Light-Induced Reactive Oxygen Species Generation and Artifactual Ca^{2+} Oscillations

A more worrying scenario is the converse explanation, namely that Ca^{2+} oscillations and spikes are actually artifacts triggered by the measurement process itself, particularly as ~30% of control experiments also show spontaneous oscillations and spikes without any stimulus. In chondrocytes, Ca^{2+} transients with a similar period (5 min) to those in guard cells are triggered by reactive oxygen species (ROS) produced by dye excitation (67). Producing ROS by strong dye illumination is sufficient to prevent progression through mitosis in plant cells (28) and may be a widespread problem in physiological measurements. The

illumination intensity at the specimen and total irradiation dose are rarely measured or reported in plant experiments. However, rates of photobleaching provide an indication of ROS production and can be assessed if the original wavelength traces are included in the results.

Fluorescence Resonance Energy Transfer-Based Metabolite Sensors

The cameleon concept has inspired the development of genetically encoded FRET-based sensors for other metabolites. Frommer and coworkers exploited the substrate-induced conformation change in bacterial periplasmic-binding proteins (PBPs) to construct FLIP sensors for maltose (33) (**Figures 1*g***, **2*j***), glucose (34, 35), ribose (76), and glutamate (101). Unlike most measurements of metabolites, these sensors report concentration directly from specific cellular compartments. As reaction rates and enzyme kinetics are concentration dependent, this should provide much better understanding of the control of metabolism in vivo. Sensitivity can be altered by mutations in the binding site and sensors can be targeted to other compartments, such as the ER (M. Fehr & W. Frommer, personal communication). The ratio change for these sensors is very small (R_{max}-R_{min} < 0.4 or R_{max}/R_{min} < 0.2). However, recent improvements include replacing EYFP with Venus (25, 101) and modifying the linker length and site of chromophore insertion to improve dipole-dipole coupling thus giving a ~twofold increase in RRC (25). Other PBP-based FRET sensors for sugars, amino acids, sulphate, and phosphate have already been synthesized using chemical coupling of fluorescent dyes (23). Incorporating the appropriate binding modules into the genetically encoded FLIP sensors should yield equivalent transgenic probes. These sensors can be expressed in plants (34), but metabolite measurements have not yet been reported.

Imaging Metabolites with Reactive Probes

In contrast to reversible binding exemplified by the cameleons, biosensors, and ratiometric ion probes, it is possible to image some metabolites, such as glutathione, ROS, or NO, following reaction in vivo to give a fluorescent product. The fluorescent signal is a cumulative measure of the amount of target molecule that reacts and is usually irreversible. Thus, reports that show decreases in fluorescence suggest interference by other processes, such as photobleaching, sequestration in a low-pH environment that quenches the fluorescence, and leakage to the medium or dye destruction by detoxification systems. If the dyes work with high efficiency, they should deplete the target molecule and interfere with the downstream pathways. For example, glutathione (GSH) concentrations can be measured in vivo following GST-catalyzed conjugation to monochlorobimane (MCB) to give a fluorescent glutathione-bimane (GSB) adduct (88). The GSB formed is transferred to the vacuole by GS-X conjugate pumps. Protocols have been developed to measure cytoplasmic GSH concentration $[GSH]_{cyt}$ in a variety of cell types (37, 38, 51, 86, 87), although imaging deep within tissues requires correction for depth-dependent attenuation (37, 51). The assay can also be used to quantify the activity of the GSH-based detoxification pathway (38) and as an indirect assay for other factors that affect GSH levels such as heavy metals, herbicides, or even explosive compounds (87, 90). The assay depletes the level of GSH and thus perturbs the system under study during the measurement. In some cases this can be used advantageously to follow the capacity of the system to respond to GSH depletion (87). Although knowledge of the total GSH pool is useful, it is perhaps more important to monitor the redox poise (GSH/GSSG ratio). Until recently this was only possible by destructive sampling and chemical analysis. However, introduction of a pair of cysteine residues (N149C and S202C) in YFP (rxYFP)

confers reversible redox-dependent changes in fluorescence (102, 103). rxYFP can be expressed in plants (P. Mullineaux, unpublished data) and is sensitive to shifts in redox state (M.D. Fricker & P. Mullineaux, unpublished data).

CONCLUSIONS

The clear drive in biology at present is to combine the predominantly reductionist approaches of the past century with the high-throughput screening technologies of this decade to provide a complete, systematic analysis. Systems biology has two components. Biologists have tended to focus on the experimental technologies used to generate vast quantities of gene, protein, and, more recently, metabolite profiles. There is a growing awareness that sophisticated data analysis tools are required to deal with these data, reflected in the rapidly expanding field of bioinformatics. What is appreciated far less is that the test of our understanding of any system at this level of complexity will be the extent to which the essential features can be captured in a mathematical model, which demands quantitative input (141). Although current "-omics" technologies excel at resolving relative amounts of different molecular species (transcripts, proteins, or metabolites), they have very poor spatial and temporal resolution. Conversely, quantitative live-cell imaging is capable of measuring amounts, concentrations, or interactions and how these change in space and time with tissue, cell, and subcellular resolution, but can typically only measure a limited, and rather restrictive, number of species simultaneously. Maximizing our understanding will require careful balancing of the strengths and weaknesses of each approach. Thus, although we envisage important roles for imaging both in setting up the precepts for model development and as a challenging environment to validate the subsequent mathematical formalization, considerable thought will be needed on how to integrate imaging effectively within systems biology. By its very nature, microscope-based imaging can only analyze a very small proportion of an individual plant and only a limited number of individuals in a population. Procedures are needed to ensure that sampling is unbiased at every level in the sampling hierarchy. Furthermore, imaging lacks an agreed standardized format for collecting, reporting, and archiving data; there are few curated and publically accessible image databases; most data is only described in qualitative terms, not least because routine quantitative analysis tools are only just beginning to become widely available, and most studies do not attempt calibration measurements with standard references (151, 152, 13a). With the explosive rise in the popularity of imaging, now would be a good time to establish appropriate guidelines to maximize the long-term value of imaging data.

ACKNOWLEDGMENTS

We would like to thank numerous colleagues for illuminating discussions during preparation of this review and apologize to the large number of authors whose work we were unable to cite fully. Research in the authors' laboratories has been supported by BBSRC (43/P19284, 43/C13425, BBS/B/03904, REI20537), NERC (GR3/12946 & NER/A/S/2002/882), EPSRC (GR/S63090/01), EU Framework 6 (STREP No. 12999), Oxford University Research Infrastructure Fund, and the University Dunston Bequest.

LITERATURE CITED

1. Achnine L, Blancaflor EB, Rasmussen S, Dixon RA. 2004. Colocalization of L-phenylalanine ammonia-lyase and cinnamate 4-hydroxylase for metabolic channeling in phenylpropanoid biosynthesis. *Plant Cell* 16:3098–109

2. Allen GJ, Chu SP, Harrington CL, Schumacher K, Hoffmann T, et al. 2001. A defined range of guard cell calcium oscillation parameters encodes stomatal movements. *Nature* 411:1053–57
3. Allen GJ, Kwak JM, Chu SP, Llopis J, Tsien RY, et al. 1999. Cameleon calcium indicator reports cytoplasmic calcium dynamics in *Arabidopsis* guard cells. *Plant J.* 19:735–47
4. Ando R, Hama H, Yamamoto-Hino M, Mizuno H, Miyawaki A. 2002. An optical marker based on the UV-induced green-to-red photoconversion of a fluorescent protein. *Proc. Natl. Acad. Sci. USA* 99:12651–56
5. Andresen M, Schmitz-Salue R, Jakobs S. 2004. Short tetracysteine tags to beta-tubulin demonstrate the significance of small labels for live cell imaging. *Mol. Biol. Cell* 15:5616–22
6. Arimura S, Yamamoto J, Aida GP, Nakazono M, Tsutsumi N. 2004. Frequent fusion and fission of plant mitochondria with unequal nucleoid distribution. *Proc. Natl. Acad. Sci. USA* 101:7805–8
7. Bastar M-T, Luthar Z, Skof S, Bohanec B. 2004. Quantitative determination of mosaic GFP gene expression in tobacco. *Plant Cell Rep.* 22:939–44
8. Benvenuto G, Formiggini F, Laflamme P, Malakhov M, Bowler C. 2002. The photomorphogenesis regulator DET1 binds the amino-terminal tail of histone H2B in a nucleosome context. *Curr. Biol.* 12:1529–34
9. Berg RH. 2004. Evaluation of spectral imaging for plant cell analysis. *J. Microsc.* 214:174–81
10. Bertrand E, Chartrand P, Schaefer M, Shenoy SM, Singer RH, Long RM. 1998. Localization of ASH1 mRNA particles in living yeast. *Mol. Cell.* 2:437–45
11. Bhat RA, Miklis M, Schmelzer E, Schulze-Lefert P, Panstruga R. 2005. Recruitment and interaction dynamics of plant penetration resistance components in a plasma membrane microdomain. *Proc. Natl. Acad. Sci. USA* 102:3135–40
12. Bornfleth H, Saetzler K, Eils R, Cremer C. 1998. High-precision distance measurements and volume-conserving segmentation of objects near and below the resolution limit in three-dimensional confocal fluorescence microscopy. *J. Microsc.* 189:118–36
13. Bracha-Drori K, Shichrur K, Katz A, Oliva M, Angelovici R, et al. 2004. Detection of protein-protein interactions in plants using bimolecular fluorescence complementation. *Plant J.* 40:419–27

13a. Brakenhoff GJ, Wurpel GWH, Jalink K, Oomen L, Brocks L, Zwier JM. 2005. Characterization of sectioning fluorescence microscopy with thin uniform fluorescent layers: Sectioned Imaging Property or SIPcharts. *J. Microsc.* 219:122–32

14. Brandizzi F, Snapp EL, Roberts AG, Lippincott-Schwartz J, Hawes C. 2002. Membrane protein transport between the endoplasmic reticulum and the Golgi in tobacco leaves is energy dependent but cytoskeleton independent: evidence from selective photobleaching. *Plant Cell* 14:1293–309

14a. Butaye KMJ, Goderis IJWM, Wouters PFJ, Pues JM-TG, Delaure SL, et al. 2004. Stable high-level transgene expression in *Arabidopsis thaliana* using gene silencing mutants and matrix attchment regions. *Plant J.* 39:440–49

15. Carlton PM, Cowan CR, Cande WZ. 2003. Directed motion of telomeres in the formation of the meiotic bouquet revealed by time course and simulation analysis. *Mol. Biol. Cell* 14:2832–43
16. Chang HY, Smertenko AP, Igarashi H, Dixon DP, Hussey PJ. 2005. Dynamic interaction of NtMAP65-1a with microtubules in vivo. *J. Cell Sci.* 118:3195–201

16a. Chapman S, Oparka KJ, Roberts AG. 2005. New tools for *in vivo* fluorescence tagging. *Curr. Op. Plant Biol.* 8:565–73

17. Chudakov DM, Verkhusha VV, Staroverov DB, Souslova EA, Lukyanov S, Lukyanov KA. 2004. Photoswitchable cyan fluorescent protein for protein tracking. *Nat. Biotechnol.* 22:1435–39
18. Chytilova E, Macas J, Sliwinska E, Rafelski SM, Lambert GM, Galbraith DW. 2000. Nuclear dynamics in *Arabidopsis thaliana*. *Mol. Biol. Cell* 11:2733–41
19. Collings DA, Carter CN, Rink JC, Scott AC, Wyatt SE, Allen NS. 2000. Plant nuclei can contain extensive grooves and invaginations. *Plant Cell* 12:2425–40
19a. Colman-Lerner A, Gordon A, Serra E, Chin T, Renekov O, et al. 2005. Regulated cell-to-cell variation in a cell-fate decision system. *Nature* 437:699–706
20. Costes SV, Daelemans D, Cho EH, Dobbin Z, Pavlakis G, Lockett S. 2004. Automatic and quantitative measurement of protein-protein colocalization in live cells. *Biophys. J.* 86:3993–4003
21. daSilva LL, Snapp EL, Denecke J, Lippincott-Schwartz J, Hawes C, Brandizzi F. 2004. Endoplasmic reticulum export sites and Golgi bodies behave as single mobile secretory units in plant cells. *Plant Cell* 16:1753–71
22. daSilva LL, Taylor JP, Hadlington JL, Hanton SL, Snowden CJ, et al. 2005. Receptor salvage from the prevacuolar compartment is essential for efficient vacuolar protein targeting. *Plant Cell* 17:132–48
23. de Lorimier RM, Smith JJ, Dwyer MA, Looger LL, Sali KM, et al. 2002. Construction of a fluorescent biosensor family. *Protein Sci.* 11:2655–75
24. Dearnaley JD, Levina NN, Lew RR, Heath IB, Goring DR. 1997. Interrelationships between cytoplasmic Ca^{2+} peaks, pollen hydration and plasma membrane conductances during compatible and incompatible pollinations of *Brassica napus* papillae. *Plant Cell Physiol.* 38:985–99
25. Deuschle K, Okumoto S, Fehr M, Looger LL, Kozhukh L, Frommer WB. 2005. Construction and optimization of a family of genetically encoded metabolite sensors by semi-rational protein engineering. *Prot. Sci.* 14:2304–14
26. Dhonukshe P, Gadella TW Jr. 2003. Alteration of microtubule dynamic instability during preprophase band formation revealed by yellow fluorescent protein-CLIP170 microtubule plus-end labeling. *Plant Cell* 15:597–611
27. Diaz I, Martinez M, Isabel-LaMoneda I, Rubio-Somoza I, Carbonero P. 2005. The DOF protein, SAD, interacts with GAMYB in plant nuclei and activates transcription of endosperm-specific genes during barley seed development. *Plant J.* 42:652–62
28. Dixit R, Cyr R. 2003. Cell damage and reactive oxygen species production induced by fluorescence microscopy: effect on mitosis and guidelines for non-invasive fluorescence microscopy. *Plant J.* 36:280–90
29. Docquier S, Tillemans V, Deltour R, Motte P. 2004. Nuclear bodies and compartmentalization of pre-mRNA splicing factors in higher plants. *Chromosoma* 112:255–66
30. Deleted in proof
31. Escobar NM, Haupt S, Thow G, Boevink P, Chapman S, Oparka K. 2003. High-throughput viral expression of cDNA-green fluorescent protein fusions reveals novel subcellular addresses and identifies unique proteins that interact with plasmodesmata. *Plant Cell* 15:1507–23
32. Fang Y, Hearn S, Spector DL. 2004. Tissue-specific expression and dynamic organization of SR splicing factors in Arabidopsis. *Mol. Biol. Cell* 15:2664–73
33. Fehr M, Frommer WB, Lalonde S. 2002. Visualization of maltose uptake in living yeast cells by fluorescent nanosensors. *Proc. Natl. Acad. Sci. USA* 99:9846–51
34. Fehr M, Lalonde S, Ehrhardt DW, Frommer WB. 2004. Live imaging of glucose homeostasis in nuclei of COS-7 cells. *J. Fluoresc.* 14:603–9

35. Fehr M, Lalonde S, Lager I, Wolff MW, Frommer WB. 2003. In vivo imaging of the dynamics of glucose uptake in the cytosol of COS-7 cells by fluorescent nanosensors. *J. Biol. Chem.* 278:19127–33
36. Franks PJ, Buckley TN, Shope JC, Mott KA. 2001. Guard cell volume and pressure measured concurrently by confocal microscopy and the cell pressure probe. *Plant Physiol.* 125:1577–84
37. Fricker MD, May M, Meyer AJ, Sheard N, White NS. 2000. Measurement of glutathione levels in intact roots of Arabidopsis. *J. Microsc.* 198:162–73
38. Fricker MD, Meyer AJ. 2001. Confocal imaging of metabolism in vivo: pitfalls and possibilities. *J. Exp. Bot.* 52:631–40
39. Gadella TW Jr, van der Krogt GN, Bisseling T. 1999. GFP-based FRET microscopy in living plant cells. *Trends Plant Sci.* 4:287–91
40. Gerlich D, Mattes J, Eils R. 2003. Quantitative motion analysis and visualization of cellular structures. *Methods* 29:3–13
41. Giege P, Heazlewood JL, Roessner-Tunali U, Millar AH, Fernie AR, et al. 2003. Enzymes of glycolysis are functionally associated with the mitochondrion in *Arabidopsis* cells. *Plant Cell* 15:2140–51
42. Goedhart J, Hink MA, Visser AJ, Bisseling T, Gadella TW Jr. 2000. In vivo fluorescence correlation microscopy (FCM) reveals accumulation and immobilization of Nod factors in root hair cell walls. *Plant J.* 21:109–19
43. Grandjean O, Vernoux T, Laufs P, Belcram K, Mizukami Y, Traas J. 2004. In vivo analysis of cell division, cell growth, and differentiation at the shoot apical meristem in *Arabidopsis*. *Plant Cell* 16:74–87
44. Gray JD, Kolesik P, Høj PB, Coombe BG. 1999. Technical advance: confocal measurement of the three-dimensional size and shape of plant parenchyma cells in a developing fruit tissue. *Plant J.* 19:229–36
45. Greer LF 3rd, Szalay AA. 2002. Imaging of light emission from the expression of luciferases in living cells and organisms: a review. *Luminescence* 17:43–74
46. Griesbeck O, Baird GS, Campbell RE, Zacharias DA, Tsien RY. 2001. Reducing the environmental sensitivity of yellow fluorescent protein. Mechanism and applications. *J. Biol. Chem.* 276:29188–94
47. Griffin BA, Adams SR, Tsien RY. 1998. Specific covalent labeling of recombinant protein molecules inside live cells. *Science* 281:269–72
48. Halfhill MD, Millwood RJ, Rufty TW, Weissinger AK, Stewart CN. 2003. Spatial and temporal patterns of green fluorescent protein (GFP) fluorescence during leaf canopy development in transgenic oilseed rape, *Brassica napus* L. *Plant Cell Rep.* 22:338–43
48a. Halpin C, Cooke SE, Barakate A, El Amrani A, Ryan MD. 1999. Self-processing 2A-polyproteins—a system for co-ordinate expression of multiple proteins in transgenic plants. *Plant J.* 17:453–59
49. Halweg C, Thompson WF, Spiker S. 2005. The Rb7 matrix attachment region increases the likelihood and magnitude of transgene expression in tobacco cells: a flow cytometric study. *Plant Cell* 17:418–29
50. Hamada S, Ishiyama K, Choi SB, Wang C, Singh S, et al. 2003. The transport of prolamine RNAs to prolamine protein bodies in living rice endosperm cells. *Plant Cell* 15:2253–64
51. Hartmann TN, Fricker MD, Rennenberg H, Meyer AJ. 2003. Cell-specific measurement of cytosolic glutathione in poplar leaves. *Plant Cell Environ.* 26:965–75
52. Haseloff J. 2003. Old botanical techniques for new microscopes. *Biotechniques* 34:1174–82

52a. Heisler MG, Ohno C, Das P, Sieber P, Reddy GV, et al. 2005. Patterns of auxin transport and gene expression during primordium development revealed by live imaging of the *Arabidopsis* inflorescence meristem. *Curr. Biol.* 15:1899–1911
53. Hetherington AM, Brownlee C. 2004. The generation of Ca^{2+} signals in plants. *Annu. Rev. Plant Biol.* 55:401–27
54. Hettinger JW, de la Pena Mattozzi M, Myers WR, Williams ME, Reeves A, et al. 2000. Optical coherence microscopy. A technology for rapid, in vivo, non-destructive visualization of plants and plant cells. *Plant Physiol.* 123:3–16
55. Hink MA, Bisseling T, Visser AJ. 2002. Imaging protein-protein interactions in living cells. *Plant Mol. Biol.* 50:871–83
56. Howard CV, Reed MG. 1998. *Unbiased Stereology: Three-Dimensional Measurement in Microscopy*. Oxford: BIOS Sci. Publ.
57. Hush JM, Wadsworth P, Callaham DA, Hepler PK. 1994. Quantification of microtubule dynamics in living plant cells using fluorescence redistribution after photobleaching. *J. Cell Sci.* 107:775–84
58. Immink RG, Gadella TW Jr, Ferrario S, Busscher M, Angenent GC. 2002. Analysis of MADS box protein-protein interactions in living plant cells. *Proc. Natl. Acad. Sci. USA* 99:2416–21
59. Iwano M, Shiba H, Miwa T, Che FS, Takayama S, et al. 2004. Ca^{2+} dynamics in a pollen grain and papilla cell during pollination of *Arabidopsis*. *Plant Physiol.* 136:3562–71
60. Jakobs S, Schauss AC, Hell SW. 2003. Photoconversion of matrix targeted GFP enables analysis of continuity and intermixing of the mitochondrial lumen. *FEBS Lett.* 554:194–200
61. Johnsson N, Johnsson K. 2003. A fusion of disciplines: chemical approaches to exploit fusion proteins for functional genomics. *Chembiochem* 4:803–10
62. Kato N, Lam E. 2001. Detection of chromosomes tagged with green fluorescent protein in live Arabidopsis thaliana plants. *Genome Biol.* 2: research0045.1–10
63. Kato N, Lam E. 2003. Chromatin of endoreduplicated pavement cells has greater range of movement than that of diploid guard cells in *Arabidopsis thaliana*. *J. Cell Sci.* 116:2195–201
64. Kato N, Pontier D, Lam E. 2002. Spectral profiling for the simultaneous observation of four distinct fluorescent proteins and detection of protein-protein interaction via fluorescence resonance energy transfer in tobacco leaf nuclei. *Plant Physiol.* 129:931–42
65. Ketelaar T, Anthony RG, Hussey PJ. 2004. Green fluorescent protein-mTalin causes defects in actin organization and cell expansion in *Arabidopsis* and inhibits actin depolymerizing factor's actin depolymerizing activity in vitro. *Plant Physiol.* 136:3990–98
66. Kluge C, Seidel T, Bolte S, Sharma SS, Hanitzsch M, et al. 2004. Subcellular distribution of the V-ATPase complex in plant cells, and in vivo localisation of the 100 kDa subunit VHA-a within the complex. *BMC Cell Biol.* 5:29
67. Knight MM, Roberts SR, Lee DA, Bader DL. 2003. Live cell imaging using confocal microscopy induces intracellular calcium transients and cell death. *Am. J. Physiol.* 284:C1083–89
68. Kohl T, Haustein E, Schwille P. 2005. Determining protease activity in vivo by fluorescence cross-correlation analysis. *Biophys. J.* 89:2770–82
69. Kohler RH, Schwille P, Webb WW, Hanson MR. 2000. Active protein transport through plastid tubules: velocity quantified by fluorescence correlation spectroscopy. *J. Cell Sci.* 113:3921–30

70. Kost B, Spielhofer P, Chua NH. 1998. A GFP-mouse talin fusion protein labels plant actin filaments in vivo and visualizes the actin cytoskeleton in growing pollen tubes. *Plant J.* 16:393–401
71. Kotzer AM, Brandizzi F, Neumann U, Paris N, Moore I, Hawes C. 2004. AtRabF2b (Ara7) acts on the vacuolar trafficking pathway in tobacco leaf epidermal cells. *J. Cell Sci.* 117:6377–89
72. Kubínová L, Janáček J, Guilak F, Opatrny Z. 1999. Comparison of several digital and stereological methods for estimating surface area and volume of cells studied by confocal microscopy. *Cytometry* 36:85–95
73. Kuner T, Augustine GJ. 2000. A genetically encoded ratiometric indicator for chloride: capturing chloride transients in cultured hippocampal neurons. *Neuron* 27:447–59
74. Kurup S, Runions J, Köhler U, Laplaze L, Hodge S, Haseloff J. 2005. Marking cell lineages in living tissues. *Plant J.* 42:444–53
75. Kwok EY, Hanson MR. 2004. GFP-labelled Rubisco and aspartate aminotransferase are present in plastid stromules and traffic between plastids. *J. Exp. Bot.* 55:595–604
76. Lager I, Fehr M, Frommer WB, Lalonde S. 2003. Development of a fluorescent nanosensor for ribose. *FEBS Lett.* 553:85–89
77. Lam E, Kato N, Watanabe K. 2004. Visualizing chromosome structure/organization. *Annu. Rev. Plant Biol.* 55:537–54
78. Landmann L. 2002. Deconvolution improves colocalization analysis of multiple fluorochromes in 3D confocal data sets more than filtering techniques. *J. Microsc.* 208:134–47
79. Levsky JM, Singer RH. 2003. Gene expression and the myth of the average cell. *Trends Cell Biol.* 13:4–6
80. Lorenzen I, Aberle T, Plieth C. 2004. Salt stress-induced chloride flux: a study using transgenic Arabidopsis expressing a fluorescent anion probe. *Plant J.* 38:539–44
81. Manders EMM, Verbeek FJ, Aten JA. 1993. Measurement of co-localization of objects in dual-colour confocal images. *J. Microsc.* 169:375–82
81a. Maple J, Aldridge C, Møller SG. 2005. Plastid division is mediated by combinatorial assembly of plastid division proteins. *Plant J.* 43:811–23
82. Mas P, Devlin PF, Panda S, Kay SA. 2000. Functional interaction of phytochrome B and cryptochrome 2. *Nature* 408:207–11
83. Mathur J, Mathur N, Hulskamp M. 2002. Simultaneous visualization of peroxisomes and cytoskeletal elements reveals actin and not microtubule-based peroxisome motility in plants. *Plant Physiol.* 128:1031–45
84. Meckel T, Hurst AC, Thiel G, Homann U. 2004. Endocytosis against high turgor: intact guard cells of *Vicia faba* constitutively endocytose fluorescently labelled plasma membrane and GFP-tagged K-channel KAT1. *Plant J.* 39:182–93
85. Messerli MA, Creton R, Jaffe LF, Robinson KR. 2000. Periodic increases in elongation rate precede increases in cytosolic Ca^{2+} during pollen tube growth. *Dev. Biol.* 222:84–98
86. Meyer AJ, Fricker MD. 2000. Direct measurement of glutathione in epidermal cells of intact *Arabidopsis* roots by two-photon laser scanning microscopy. *J. Microsc.* 198:174–81
87. Meyer AJ, Fricker MD. 2002. Control of demand-driven biosynthesis of glutathione in green Arabidopsis suspension culture cells. *Plant Physiol.* 130:1927–37
88. Meyer AJ, May MJ, Fricker M. 2001. Quantitative in vivo measurement of glutathione in Arabidopsis cells. *Plant J.* 27:67–78
89. Meyers BC, Galbraith DW, Nelson T, Agrawal V. 2004. Methods for transcriptional profiling in plants. Be fruitful and replicate. *Plant Physiol.* 135:637–52

90. Mezzari MP, Walters K, Jelinkova M, Shih MC, Just CL, Schnoor JL. 2005. Gene expression and microscopic analysis of *Arabidopsis* exposed to chloroacetanilide herbicides and explosive compounds. A phytoremediation approach. *Plant Physiol.* 138:858–69
91. Mirabella R, Franken C, van der Krogt GN, Bisseling T, Geurts R. 2004. Use of the fluorescent timer DsRED-E5 as reporter to monitor dynamics of gene activity in plants. *Plant Physiol.* 135:1879–87
92. Miyawaki A, Griesbeck O, Heim R, Tsien RY. 1999. Dynamic and quantitative Ca^{2+} measurements using improved cameleons. *Proc. Natl. Acad. Sci. USA* 96:2135–40
93. Miyawaki A, Llopis J, Heim R, McCaffery JM, Adams JA, et al. 1997. Fluorescent indicators for Ca^{2+} based on green fluorescent proteins and calmodulin. *Nature* 388:882–87
94. Moriguchi K, Suzuki T, Ito Y, Yamazaki Y, Niwa Y, Kurata N. 2005. Functional isolation of novel nuclear proteins showing a variety of subnuclear localizations. *Plant Cell* 17:389–403
95. Nagai T, Yamada S, Tominaga T, Ichikawa M, Miyawaki A. 2004. Expanded dynamic range of fluorescent indicators for Ca^{2+} by circularly permuted yellow fluorescent proteins. *Proc. Natl. Acad. Sci. USA* 101:10554–59
96. Nakajima K, Sena G, Nawy T, Benfey PN. 2001. Intercellular movement of the putative transcription factor SHR in root patterning. *Nature* 413:307–11
97. Nebenführ A, Gallagher LA, Dunahay TG, Frohlick JA, Mazurkiewicz AM, et al. 1999. Stop-and-go movements of plant Golgi stacks are mediated by the acto-myosin system. *Plant Physiol.* 121:1127–42
98. Neher R, Neher E. 2004. Optimizing imaging parameters for the separation of multiple labels in a fluorescence image. *J. Microsc.* 213:46–62
99. Ng CKY, McAinsh MR. 2003. Encoding specificity in plant calcium signalling: Hotspotting the ups and downs and waves. *Ann. Bot.* 92:477–85
100. Okita TW, Choi SB. 2002. mRNA localization in plants: targeting to the cell's cortical region and beyond. *Curr. Opin. Plant Biol.* 5:553–59
101. Okumoto S, Looger LL, Micheva KD, Reimer RJ, Smith SJ, Frommer WB. 2005. Detection of glutamate release from neurons by genetically encoded surface-displayed FRET nanosensors. *Proc. Natl. Acad. Sci. USA* 102:8740–45
102. Østergaard H, Henriksen A, Hansen FG, Winther JR. 2001. Shedding light on disulfide bond formation: engineering a redox switch in green fluorescent protein. *EMBO J.* 20:5853–62
103. Østergaard H, Tachibana C, Winther JR. 2004. Monitoring disulfide bond formation in the eukaryotic cytosol. *J. Cell Biol.* 166:337–45
104. Patterson GH, Lippincott-Schwartz J. 2002. A photoactivatable GFP for selective photolabeling of proteins and cells. *Science* 297:1873–77
105. Pecinka A, Kato N, Meister A, Probst AV, Schubert I, Lam E. 2005. Tandem repetitive transgenes and fluorescent chromatin tags alter local interphase chromosome arrangement in Arabidopsis thaliana. *J. Cell Sci.* 118:3751–58
106. Pecinka A, Schubert V, Meister A, Kreth G, Klatte M, et al. 2004. Chromosome territory arrangement and homologous pairing in nuclei of Arabidopsis thaliana are predominantly random except for NOR-bearing chromosomes. *Chromosoma* 113:258–69
107. Pesquet E, Barbier O, Ranocha P, Jauneau A, Goffner D. 2004. Multiple gene detection by in situ RT-PCR in isolated plant cells and tissues. *Plant J.* 39:947–59
108. Pierson ES, Miller DD, Callaham DA, Van AJ, Hackett G, Hepler PK. 1996. Tip-localized calcium entry fluctuates during pollen tube growth. *Dev. Biol.* 174:160–73

109. Plieth C. 2005. Calcium: just another regulator in the machinery of life? *Ann. Bot.* 96:1–8
110. Reddy GV, Heisler MG, Ehrhardt DW, Meyerowitz EM. 2004. Real-time lineage analysis reveals oriented cell divisions associated with morphogenesis at the shoot apex of *Arabidopsis thaliana*. *Development* 131:4225–37
110a. Reddy GV, Meyerowitz EM. 2005. Stem-cell homeostasis and growth dynamics can be uncoupled in the *Arabidopsis* shoot apex. *Science* 310:663–67
111. Reeves A, Parsons RL, Hettinger JW, Medford JI. 2002. In vivo three-dimensional imaging of plants with optical coherence microscopy. *J. Microsc.* 208:177–89
112. Runions J, Brach T, Kuhner S, Hawes C. 2005. Photoactivation of GFP reveals protein dynamics within the endoplasmic reticulum membrane. *J. Exp. Bot.* doi:10.1093/jxb/eri289
113. Russinova E, Borst JW, Kwaaitaal M, Cano-Delgado A, Yin Y, et al. 2004. Heterodimerization and endocytosis of Arabidopsis brassinosteroid receptors BRI1 and AtSERK3 (BAK1). *Plant Cell* 16:3216–29
114. Schwille P, Haupts U, Maiti S, Webb WW. 1999. Molecular dynamics in living cells observed by fluorescence correlation spectroscopy with one- and two-photon excitation. *Biophys. J.* 77:2251–65
115. Scrase-Field SAMG, Knight MR. 2003. Calcium: just a chemical switch? *Curr. Opin. Plant Biol.* 6:500–6
116. Shah K, Gadella TW Jr, van Erp H, Hecht V, de Vries SC. 2001. Subcellular localization and oligomerization of the *Arabidopsis thaliana* somatic embryogenesis receptor kinase 1 protein. *J. Mol. Biol.* 309:641–55
117. Shah K, Russinova E, Gadella TW Jr, Willemse J, De Vries SC. 2002. The *Arabidopsis* kinase-associated protein phosphatase controls internalization of the somatic embryogenesis receptor kinase 1. *Genes Dev.* 16:1707–20
118. Sharpe J, Ahlgren U, Perry P, Hill B, Ross A, et al. 2002. Optical projection tomography as a tool for 3D microscopy and gene expression studies. *Science* 296:541–45
119. Shaw SL, Kamyar R, Ehrhardt DW. 2003. Sustained microtubule treadmilling in *Arabidopsis* cortical arrays. *Science* 300:1715–18
120. Sheahan MB, Staiger CJ, Rose RJ, McCurdy DW. 2004. A green fluorescent protein fusion to actin-binding domain 2 of *Arabidopsis* fimbrin highlights new features of a dynamic actin cytoskeleton in live plant cells. *Plant Physiol.* 136:3968–78
121. Shope JC, DeWald DB, Mott KA. 2003. Changes in surface area of intact guard cells are correlated with membrane internalization. *Plant Physiol.* 133:1314–21
121a. Sohn EJ, Kim ES, Zhao M, Kim SJ, Kim H, et al. 2003. Rha1, an Arabidopsis Rab5 homolog, plays a critical role in the vacuolar trafficking of soluble cargo proteins. *Plant Cell* 15:1057–70
122. Sprague BL, McNally JG. 2005. FRAP analysis of binding: proper and fitting. *Trends Cell Biol.* 15:84–91
123. Stadler R, Wright KM, Lauterbach C, Amon G, Gahrtz M, et al. 2005. Expression of GFP-fusions in Arabidopsis companion cells reveals non-specific protein trafficking into sieve elements and identifies a novel post-phloem domain in roots. *Plant J.* 41:319–31
124. Subramaniam R, Desveaux D, Spickler C, Michnick SW, Brisson N. 2001. Direct visualization of protein interactions in plant cells. *Nat. Biotechnol.* 19:769–72
125. Subramanian C, Kim BH, Lyssenko NN, Xu X, Johnson CH, von Arnim AG. 2004. The Arabidopsis repressor of light signaling, COP1, is regulated by nuclear exclusion: mutational analysis by bioluminescence resonance energy transfer. *Proc. Natl. Acad. Sci. USA* 101:6798–802

126. Subramanian C, Xu Y, Johnson CH, von Arnim AG. 2004. In vivo detection of protein-protein interaction in plant cells using BRET. *Methods Mol. Biol.* 284:271–86
127. Swarup R, Kargul J, Marchant A, Zadik D, Rahman A, et al. 2004. Structure-function analysis of the presumptive Arabidopsis auxin permease AUX1. *Plant Cell* 16:3069–83
128. Tamura K, Shimada T, Ono E, Tanaka Y, Nagatani A, et al. 2003. Why green fluorescent fusion proteins have not been observed in the vacuoles of higher plants. *Plant J.* 35:545–55
129. Terskikh A, Fradkov A, Ermakova G, Zaraisky A, Tan P, et al. 2000. "Fluorescent timer": protein that changes color with time. *Science* 290:1585–88
130. Tour O, Meijer RM, Zacharias DA, Adams SR, Tsien RY. 2003. Genetically targeted chromophore-assisted light inactivation. *Nat. Biotechnol.* 21:1505–8
131. Tsien RY. 2005. Building and breeding molecules to spy on cells and tumors. *FEBS Lett.* 579:927–32
131a. Tsutsui H, Karasawa S, Shimizu H, Nukina N, Miyawaki A. 2005. Semi-rational engineering of a coral fluorescent protein into an efficient highlighter. *EMBO Rep.* 6:233–38
131b. Ueda T, Uemura T, Sato MH, Nakano A. 2004. Functional differentiation of endosomes in Arabidopsis cells. *Plant J.* 40:783–89
132. Van Bruaene N, Joss G, Thas O, Van Oostveldt P. 2003. Four-dimensional imaging and computer-assisted track analysis of nuclear migration in root hairs of *Arabidopsis thaliana*. *J. Microsc.* 211:167–78
133. Verkhusha VV, Sorkin A. 2005. Conversion of the monomeric red fluorescent protein into a photoactivatable probe. *Chem. Biol.* 12:279–85
134. Vermeer JE, Van Munster EB, Vischer NO, Gadella TW Jr. 2004. Probing plasma membrane microdomains in cowpea protoplasts using lipidated GFP-fusion proteins and multimode FRET microscopy. *J. Microsc.* 214:190–200
135. Vogel H, Grieninger GE, Zetsche KH. 2002. Differential messenger RNA gradients in the unicellular alga *Acetabularia acetabulum*. Role of the cytoskeleton. *Plant Physiol.* 129:1407–16
136. Voon DC, Subrata LS, Baltic S, Leu MP, Whiteway JM, et al. 2005. Use of mRNA- and protein-destabilizing elements to develop a highly responsive reporter system. *Nucleic Acids Res.* 33:e27
137. Walter M, Chaban C, Schutze K, Batistic O, Weckermann K, et al. 2004. Visualization of protein interactions in living plant cells using bimolecular fluorescence complementation. *Plant J.* 40:428–38
138. Wang YS, Motes CM, Mohamalawari DR, Blancaflor EB. 2004. Green fluorescent protein fusions to *Arabidopsis fimbrin* 1 for spatio-temporal imaging of F-actin dynamics in roots. *Cell Motil. Cytosk*eleton 59:79–93
139. Ward TH, Brandizzi F. 2004. Dynamics of proteins in Golgi membranes: comparisons between mammalian and plant cells highlighted by photobleaching techniques. *Cell. Mol. Life Sci.* 61:172–85
140. Watahiki MK, Trewavas AJ, Parton RM. 2004. Fluctuations in the pollen tube tip-focused calcium gradient are not reflected in nuclear calcium levels: a comparative analysis using recombinant yellow cameleon calcium reporter. *Sex. Plant Reprod.* 17:125–30
141. Westerhoff HV, Palsson BO. 2004. The evolution of molecular biology into systems biology. *Nat. Biotechnol.* 22:1249–52
142. White NS, Errington RJ, Fricker MD, Wood JL. 1996. Aberration control in quantitative imaging of botanical specimens by multidimensional fluorescence microscopy. *J. Microsc.* 181:99–116

142a. Wiedenmann J, Ivanchenko S, Oswald F, Schmitt F, Röcker C, et al. 2004. EosFP, a fluorescent marker protein with UV-inducible green-to-red fluorescence conversion. *Proc. Natl. Acad. Sci. USA* 101:15905–10

143. Worley CK, Ling R, Callis J. 1998. Engineering in vivo instability of firefly luciferase and *Escherichia coli* beta-glucuronidase in higher plants using recognition elements from the ubiquitin pathway. *Plant Mol. Biol.* 37:337–47

143a. Wu J-Q, Pollard TD. 2005. Counting cytokinesis proteins globally and locally in fission yeast. *Science* 310:310–14

144. Yamaguchi R, Nakamura M, Mochizuki N, Kay SA, Nagatani A. 1999. Light-dependent translocation of a phytochrome B-GFP fusion protein to the nucleus in transgenic *Arabidopsis*. *J. Cell Biol.* 145:437–45

144a. Yamamoto YY, Tsuhara Y, Gohda K, Suzuki K, Matsui M. 2003. Gene trapping of the *Arabidopsis* genome with a firefly luciferase reporter. *Plant J.* 35:273–83

145. Yang YD, Elamawi R, Bubeck J, Pepperkok R, Ritzenthaler C, Robinson DG. 2005. Dynamics of COPII vesicles and the Golgi apparatus in cultured *Nicotiana tabacum* BY-2 cells provides evidence for transient association of Golgi stacks with endoplasmic reticulum exit sites. *Plant Cell* 17:1513–31

146. Yoo BC, Kragler F, Varkonyi-Gasic E, Haywood V, Archer-Evans S, et al. 2004. A systemic small RNA signaling system in plants. *Plant Cell* 16:1979–2000

147. Zhang F, Simon AE. 2003. A novel procedure for the localization of viral RNAs in protoplasts and whole plants. *Plant J.* 35:665–73

148. Zheng H, Camacho L, Wee E, Batoko H, Legen J, et al. 2005. A Rab-E GTPase mutant acts downstream of the Rab-D subclass in biosynthetic membrane traffic to the plasma membrane in tobacco leaf epidermis. *Plant Cell* 17:2020–36

149. Zhou X, Carranco R, Vitha S, Hall TC. 2005. The dark side of GFP. *New Phytol.* 168:313–21

150. Zimmermann T, Rietdorf J, Pepperkok R. 2003. Spectral imaging and its applications in live cell microscopy. *FEBS Lett.* 546:87–92

151. Zucker RM, Price O. 2001. Evaluation of confocal microscopy system performance. *Cytometry* 44:273–94

152. Zucker RM, Price OT. 2001. Statistical evaluation of confocal microscopy images. *Cytometry* 44:295–308